Soft Matter

Accepted Manuscript

ROYAL SOCIETY OF CHEMISTRY

rsc.li/soft-matter-journal

Journal Name

Influence of Macromolecular Crowding in the Charge Regulation of Intrinsically Disordered Proteins[†]

Pablo M. Blanco,[a,*] Sergio Madurga,[a] Josep L. Garcés,[b] Francesc Mas[a,*] and Rita S. Dias[c,*]

In this work we study the coupling between ionization and conformational properties of two IDPs, histatin-5 and β-amyloid 42, in the presence of neutral and charged crowders. The latter are modeled to resemble Bovin Serum Albumin (BSA). With this aim, Semi-Grand Canonical Monte Carlo simulations are performed, so that the IDPs charge is a dynamic property, undergoing protonation/deprotonation processes. Both ionization properties (global and specific aminoacid charge, binding capacitance) and radius of gyration are analyzed in a large range of pH values and salt concentrations. Without crowder agents, the titration curve of histatin-5, a polycation, is salt-dependent while that of β-amyloid 42, a polyampholyte, is almost unaffected. The salt concentration is found to be specially relevant at pH values where the protein binding capacitance (directly linked with charge fluctuation) is larger. Upon addition of neutral crowders, charge regulation is observed in histatin-5, while for β-amyloid 42 this effect is very small. The main mechanism for charge regulation is found to be the effective increase in the ionic strenght due to excluded volume. In presence of charged crowders, significant increase in the charge of both IDPs is observed at almost all the pH range. In this case, the IDP charge is altered not only by the increase in the effective ionic strength but also by its direct electrostatic interaction with the charged crowders.

1 Introduction

For many years, the basis of enzymatic biochemistry were laid following the classic "lock-and-key" principle, which relates the specific conformation of an enzyme with its biological function.[1] Under this paradigm, and despite their abundance in all proteomes, proteins with partially or entirely disordered sequences, the so-called Intrinsically Disordered Proteins (IDPs), were considered to have no specific biologic role or simply that of connecting ordered domains[2,3]. Nowadays, however, the characteristic structural flexibility of IDPs has been found to exhibit many biological advantages such as multi-binding, the capability to avoid non-desired interactions through functional misfolding,[4] or overcoming steric restrictions due to macromolecular crowding[5]. Due to these advantages, IDPs are involved in a wide spectra of biological processes[6], such as signalling processes, supramolecular assembly or allosteric regulation, so that they are appealing targets for drugs.

On the other side, biological media are highly concentrated in macromolecular species, the so-called macromolecular crowding[7,8]. For instance, the weight fraction of protein in blood plasma is around 9%, with serum albumin being the most abundant protein with concentration around 35-55 g/L[9]. In the cell cytosol, macromolecules occupy a volume fraction of 20%-40%, with approximate macromolecule concentrations 200–400 g/L. The impact of macromolecular crowding in proteins with a defined 3D structure has been extensively studied; it has been found to substantially affect the reactivity, conformational properties,

[a] Physical Chemistry Unit, Materials Science and Physical Chemistry Department & Research Institute of Theoretical and Computational Chemistry (IQTCUB) of Barcelona University (UB), Barcelona (Catalonia, Spain) E-mail: pmblanco23@gmail.com; fmas@ub.edu

[b] Chemistry Department. Technical School of Agricultural Engineering & AGROTECNIO of Lleida University (UdL), Lleida (Catalonia, Spain).

[c] Department of Physics, Norwegian University of Science and Technology (NTNU), Trondheim (Norway) E-mail: rita.dias@ntnu.no

† Electronic Supplementary Information (ESI) available: Additional graphics that can be found as part of the supporting information: (S1) Charge and binding capacitance per aminoacid vs. pH in dilute solution; (S2) Variation of the charge of aspartic acid, histidine and lysine due to the added salt vs. pH in dilute solution; (S3) Charge variation vs. pH for the case with neutral crowders with salt concentration 0.01 M; (S4) Variation of the IDP global charge vs. excluded volume (S5) Binding capacitance per aminoacid vs. pH for the case with neutral crowders with salt concentration 0.1 M; (S6) Best fit parameters to the scaling law (Eq. 13) for the R_g vs. ϕ curves (S7) Binding capacitance per aminoacid vs. pH for the case with charged crowders with salt concentration 0.01 M; (S8) Calculations with effective ionic strength I' for the case with charged crowders; and (S9) Comparison of $\Delta Q(c_s)$ and $\Delta Q'(\phi)$ vs. pH for systems with $I' = 0.05$ M.

diffusion processes and self-assembly[7,8,10–22]. In the case of IDPs, the latter point is specially relevant to unravel their physiological role and to prevent the pathways that lead to unwanted self-association or association of these proteins with other macromolecules.

Research on the response of IDPs to macromolecular crowding has been mainly focused on their conformational properties. Macromolecular crowding effect in the conformational properties of IDPs has been found to be rather heterogeneous and, in general, it is dependent on each IDP-crowder combination[23–27]. Therefore, IDPs have been classified as foldable (fold upon crowding), unfoldable (extended upon crowding) and non-foldable (mostly unaffected)[5]. This variability suggests that the impact of molecular crowding on IDPs is not only due to the excluded volume effect, but that other variables, such as the macromolecular charge, could also play a key role. For example, the presence of crowders may alter the conformation of the protein, which in turn affects the ionization state of the weak acid/base groups of the protein.

Coupling between conformational and ionization properties has been reported to be significant in IDPs[28,29] and it is a rather general trend of weak polyelectrolytes[30–36]. Some examples are the swelling of poly(methacrylic) acid in a narrow range of pH[37], the important influence of ionization in protein folding[38] or the helix–coil transitions of poly(peptides)[39]. The ability of a macromolecule to modulate its charge as a response to an external stimulus (e.g. pH variations, salt concentration changes, interactions with other macromolecules or external fields) is known as Charge Regulation[40,41]. This capability has lead to the use of weak polyelectrolytes in pH-responsive smart systems with multiple technological applications (see, for instance, Ref.[42] and references quoted therein).

Moreover, both IDPs and weak polyelectrolytes possess a very flexible structure so that simulation techniques borrowed from weak polyelectrolytes can be straightforwardly used in modeling IDPs. In particular, "bead-and-spring" models[32,34–36,43–49] have been successfully used to simulate IDPs[50–52]. Using Monte Carlo simulations of this nature, Skepö et al. have been able to reproduce small-angle X-ray scattering[52,53] and ellipsometry[50,51] experiments. Furthermore, in both cases ionization equilibria can be explicitly taken into account by using Monte Carlo simulations in the Semi-Grand Canonical Monte Carlo ensemble[32,34–36,54,55].

In this work we will focus on the effect of macromolecular crowding on charge regulation and conformational structure of two IDPs with very different biological functions: histatin-5 and β-amyloid 42. Histatin-5 is present in human saliva[50–53] and presents antibacterial[56], antifungal[57,58], and polyphenolic-binding[59,60] properties. β-amyloid 42 is known for its ability to self-assemble, forming fibres in the brain of patients with Alzheimer disease[61–63]. This article is organised as follows. In section two, the theoretical model, its parameterization and the computational details are introduced. Following a step-wise approach, we analyse in section three the ionization and conformational properties of the IDPs in the (i) absence of crowding agents; (ii) presence of neutral crowders, and (iii) presence of charged crowders.

2 Methodology

Histatin-5 and β-amyloid 42 present a rather different ionization properties: Histatin-5 is a polycation while β-amyloid 42 is a polyampholyte. In this work they are modelled using a simple bead-and-spring model. The conformational and ionization properties are computed by means of Semi-Grand Canonical Monte Carlo simulations using MOLSIM software[64]. The crowders are described by means of the recently developed Chain Entanglement Softened Potential (CESP) model[21]. Within this model, they are regarded as double-shelled spheres with an inner hard-core and an outer soft shell. In order to evaluate the effect of the crowder agents, we perform simulations with charged and uncharged crowders. When considered, the crowders charge is fixed at a given pH, and modelled by placing charged beads at the sphere surface. Therefore, only the IDP charge is allowed to fluctuate. In Fig. 1, two examples of the performed simulations are shown. In the left upper panel we have depicted β-amyloid 42 in a solution of neutral crowders (cyan double-shelled spheres) occupying a large fraction of the volume. In the right-hand side upper panel the solution contains histatin-5 and charged crowders (cyan double-shelled spheres with blue beads in its surface representing the charges). The chemical species in solution, as well as the different models used, are outlined in the bottom panel of Fig. 1. Let us discuss in detail the methods used in this work.

2.1 Theoretical model

For simplicity, let us consider the case in which only one IDP chain is present in a medium populated by crowder macromolecules and salt ions. The atomistic modeling of this medium is computationally challenging due to the massive quantity of atoms in solution and the physicochemical processes involved. Our model aims to reduce the system complexity while retaining the most relevant physicochemical aspects (electrostatic interactions and steric hinderance) involved in the acid/base equilibria of the IDP. We make use of a multi-layered coarse-grained description with different degrees of detail depending on the chemical identity of each component, as outlined in Fig. 1.

The IDP chain is described as a set of M beads joined by elastic bonds. The bonds are approximated as springs with a harmonic potential

$$F_B = \frac{k_{\text{Bond}}}{2} \sum_{j=1}^{M-1} (l_j - l_0)^2, \tag{1}$$

where l_j is the length of bond j, l_0 is the bond equilibrium length and k_{Bond} is the harmonic force constant. Each bead represents an aminoacid residue and two extra beads are used to describe the terminal amino/carboxylic groups, as depicted in Fig. 1. The beads holding an acid/base group are allowed to change their ionization state, mimicking proton binding/unbinding. For a protein chain with S acid/basic beads, the protonation free energy F_P reads[32,34–36,67]

$$\frac{\beta F_P}{\ln(10)} = \sum_{i=1}^{S} \mu_i s_i = \sum_{i=1}^{S} (\text{pH} - \text{p}K_{a,i}) s_i, \tag{2}$$

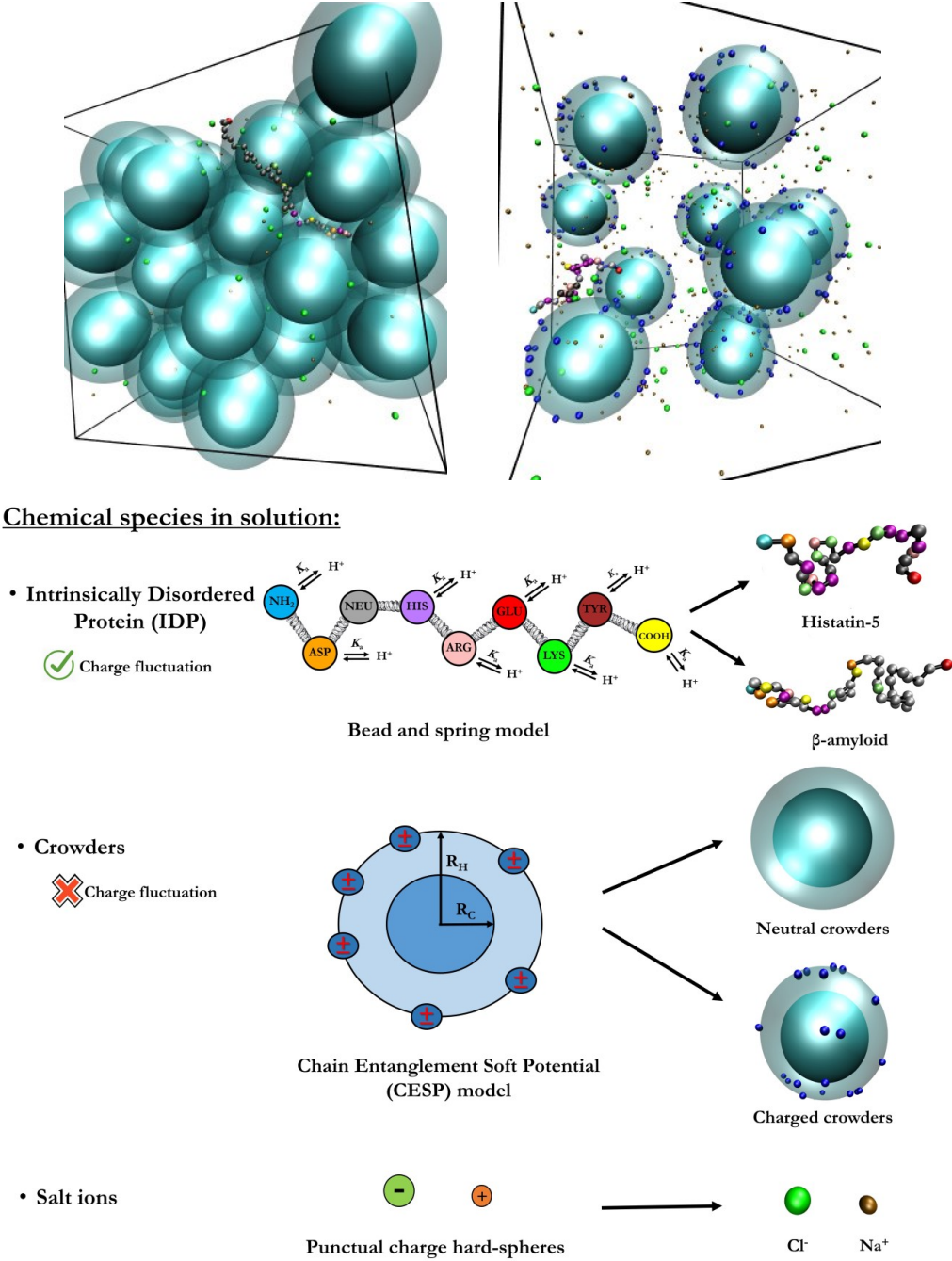where $\text{pH} = -\log(a_H)$ depends on the proton activity a_H, $\beta =$

Fig. 1 Upper panel: two snapshots of Semi-Grand Canonical Monte Carlo simulations of: (left) β-amyloid 42 in a medium containing neutral crowders with excluded volume fraction $\phi = 0.39$ and (right) histatin-5 surrounded by charged crowders with $\phi = 0.08$. Bottom panel: Outline of the chemical species in solution. Both IDPs (coloured chain) are modeled by means of a bead and spring model[50–52], with acid/base equilibria explicitly taken into account. The crowders (cyan double-shelled spheres) are modeled using the Chain Entanglement Softened Potential (CESP) model[21], for which the crowders have an inner dense core (opaque) and an outer softer region (transparent). In the case of charged crowders, small charged beads (blue) are added mimicking the Bovin Serum Albumin surface charge. Na^+ (orange spheres) and Cl^- (green spheres) ions are also present with concentration of 0.01 M.

Particle	-ARG-	-LYS-	-TYR-	-HIS-	-GLU-	-ASP-	$-NH_2$	-COOH
$pK_{a,i}$	12.0	10.4	9.6	6.3	4.4	4.0	7.5	3.8

Table 1 pK_a-values for the titrable aminoacid residues and for the terminal amino ($-NH_2$) and carboxylic (-COOH) groups, obtained from Ref.[66]

Histatin-5 sequence: (24 aminoacids: **15 basic** and **5 acid** groups)

NH$_2$ – ASP – SER – HIS – ALA – LYS – ARG – HIS – HIS – GLY – TYR – LYS – ARG – LYS –

– PHE – HIS – GLU – LYS – HIS – HIS – SER – HIS – ARG – GLY – TYR – COOH

B-amyloid 42 sequence: (42 aminoacids: **7 basic** and **8 acid** groups)

NH$_2$ – ASP – ALA – GLU – PHE – ARG – HIS – ASP – SER – GLY – TYR – GLU – VAL – HIS –

– HIS – GLN – LYS – LEU – VAL – PHE – PHE – ALA – GLU – ASP – VAL – GLY – SER –

– ASN – LYS – GLY – ALA – ILE – ILE – GLY – LEU – MET – VAL – GLY – GLY – VAL –

– VAL – ILE – ALA – COOH

Fig. 2 Aminoacid sequence of Histatin-5[50,65] and β-amyloid 42[61]. The amino acids with basic and acid groups are coloured in blue and red, respectively.

$1/(k_\text{B}T)$ is the inverse of the thermal energy with k_B the Boltzmann constant and T the temperature. For a given ionizable group i, μ_i and p$K_{\text{a},i}$ represent its reduced chemical potential and its acid constant, respectively. s_i is a variable representing its protonation state, whose value can be either 1 (protonated) or 0 (unprotonated).

The crowders are modelled using the recently developed Chain Entanglement Softened Potential (CESP) model[21]. In this model, the particles interact through an empiric inter-particle interaction potential containing a continuous shouldered well, similar to that used in computational models of coarse-grained fluids[68,69]. The particle is divided into two distinct regions: (i) the core, which is densely populated by atoms and modeled as a hard-sphere of radius R_C, and (ii) the outer part, in contact with the solvent, which is less dense and can be penetrated by other particles with energetic cost U_r. Its radius is estimated as the hydrodynamic radius of the macromolecule R_H, as depicted in Fig. 1. The mean-field pair-wise potential, F_CESP, corresponding to this model, is given by the empirical expression

$$F_\text{CESP} = \sum_{i,j}^{N} \varepsilon_0 \left(\frac{d_\text{C}}{d_{ij}}\right)^{24} - \frac{U_r}{2} \tanh\left(\frac{d_C/d_0}{d_E - d_C}\left(d_{ij} - \frac{d_E + d_C}{2}\right)\right) + \frac{U_r}{2}$$

(3)

where d_{ij} is the distance between the centers of the interacting particles i and j. $\varepsilon_0 = 1$ J mol^{-1} and $d_0 = 1$ nm are added to correct the units[21] while $d_\text{C} = R_{\text{C},i} + R_{\text{C},j}$ and $d_\text{H} = R_{\text{H},i} + R_{\text{H},j}$ represent the sum of hard core and hydrodynamic radii of particles i and j, respectively. Conversely, the steric repulsion between protein beads, ions and between beads and ions is calculated only using the first, repulsive, term in Eq. 3.

The electrostatic interaction in the implicit solvent assumption obeys the Coulomb potential

$$\beta F_\text{C} = \sum_{i=1}^{N} \sum_{j=i+1}^{N} \frac{\ell_\text{B}}{d_{ij}} q_i q_j$$

(4)

where ℓ_B is the Bjerrum length, which is $\ell_\text{B} \simeq 0.71$ nm at 298 K.

The total free energy of the system reads

$$F = F_\text{B} + F_\text{P} + F_\text{CESP} + F_\text{C}.$$

(5)

2.2 Parameterization

The aminoacid sequences of histatin-5 and β-amyloid 42 can be found in Fig. 2. Both IDPs are short peptide chains with a flexible random-coil structure but they exhibit very different acid/base properties. Histatin-5 consists of a large number of basic aminoacids (mainly histidine), so it is positively charged in a wide range of pH-values. β-amyloid 42, on the other hand, presents almost the same number of acid and basic aminoacids, so its charge undergoes a transition from positive at low pH-values to negative at high pH-values. Inspired by the model suggested by Skepö *et al.*, we describe aminoacid residues as beads with hard-core radius $R_\text{C} = 0.2$ nm[50–53]. There are also two extra beads for the terminal amino/carboxylic groups with the same radius $R_\text{C} = 0.2$ nm. The aminoacids hard-core and hydrodynamic radii are taken to be equal. The beads are joined by harmonic bonds with equilibrium bond length $l_0 = 0.41$ nm and force constant $k_\text{Bond} = 240$ kJ mol^{-1}nm^{-2} or 0.4 N m^{-1}. The intrinsic acid constants (p$K_{\text{a},i}$) of the aminoacids are taken from Ref.[66] and can be also found in Tab. 1.

Aiming to mimic a biologically realistic scenario, the crowders have been chosen to resemble Bovine Serum Albumin (BSA). We have chosen BSA instead of its human variant because it has been more extensively used in research and it is thus better parameterized. Since we are also interested in the effect of the crowder charge, we firstly study the simpler situation of neutral crowders with the same dimensions as BSA. The hard-core radius R_C can be estimated as[21]

$$R_\text{C}(\text{BSA}) = \sqrt[3]{\frac{3\nu M_\text{W}}{4\pi N_\text{A}}} = 2.73 \text{ nm},$$

(6)

where $\nu = 0.736$ cm^{3}g^{-1} and $M_\text{W} = 70$ kg mol^{-1} are the specific volume[71] and the molecular weight[72] of BSA, respectively, and N_A is the Avogadro constant. R_H is calculated using the Stokes-

Soft Matter Accepted Manuscript

pH	3.00	3.50	4.00	4.50	4.65	5.00	6.00	7.00	8.00	9.00	10.0	11.0
Net charge/e	+22	+18	+10	+6	0	-4	-9	-15	-19	-22	-26	-27

Table 2 Average net charge of Bovine Serum Albumin (BSA) at different pH values. The values were obtained from capillary electrophoresis by measuring the electrophoretic mobility of BSA[70].

Einstein equation

$$R_{\mathrm{H}}(\mathrm{BSA}) = \frac{k_{\mathrm{B}}T}{6\pi\eta D} = 3.64 \text{ nm} , \qquad (7)$$

where $\eta = 0.932$ mPa is water viscosity at room temperature[73]. $D = 6.32 \cdot 10^{-2}$ nm^{2}ns^{-1} represents the BSA translational diffusion coefficient at 293 K, obtained from dynamic light scattering[74] and quasi-elastic light scattering[75] experiments at pH = 5, near the isolectric point of BSA (pH $\simeq 4.65$)[70]. Although the diffusion coefficient of BSA slightly varies with the pH-value[74] (which leads to different R_{H} values ranging from 4.29 nm for pH = 3 to 3.53 nm for pH = 7), we will consider, for simplicity, the size of BSA to be pH-independent. The entanglement energetic cost U_{r} has been determined in a recent publication[21] to be $U_{\mathrm{r}} = 5000$ J mol^{-1} by fitting brownian dynamic simulations using CESP potential (Eq. 3) to experimental long-time diffusion coefficients. This value prevents crowders to overlap at low concentrations while it allows crowder-particle inter-crossing at high crowder concentrations.

In the simulations with charged crowders, we have to account for the fact that the net charge of the BSA is sensitive to the pH of the medium. One could in principle treat explicitly the ionization equilibrium of BSA and the consequent charge fluctuations. However, this turns to be computationally very expensive. We have thus decided to assign charge to the charged crowders according to the solution pH and keep it constant during the simulations, i.e., charge regulation is included in the IDPs but not in charged crowders. The net charge of BSA for different pH values was obtained from capillary electrophoresis experimental data[70] and can be found in Tab. 2. It is distributed in hard-sphere beads with $R_{\mathrm{C}} = 0.2$ nm containing one elementary charge, which are randomly placed at the surface of the crowders (at a distance R_{H} from the center, see Fig. 1). Previous works have pointed out the relevance of the charge distribution in protein-polyelectrolyte interactions[76–80]. This is not the case of our system, where preliminary calculations showed no significant effect of the charge distribution of the crowders in the conformational and ionization properties of the IDPs. This difference is possibly due to the fact that polyelectrolytes, in general, have larger charge densities than IDPs. For a given pH-value, all the crowders are considered to have equal charge distribution. In order to avoid anisotropy problems, the crowders are allowed to rotate during the simulation.

Finally, the electroneutrality of the solution is ensured by adding the appropriate amount of sodium Na$^+$ and chloride Cl$^-$ ions, also modeled as hard spheres with radii equal to its ionic radii: $R_{\mathrm{C}}(\mathrm{Na}^+) = 0.10$ nm and $R_{\mathrm{C}}(\mathrm{Cl}^-) = 0.18$ nm[81–83].

2.3 Computational details

Semi-Grand Canonical Monte Carlo simulations[32,34–36,54,55] were performed using MOLSIM v6.4.7 software[64]. An additional routine with the CESP contribution to the free energy was added to the original MOLSIM code. The routine was tested by reproducing the results presented in Ref.[21]. The simulations were performed at room temperature $T = 298.15$ K in a cubic simulation box with a side length $L = 22$ nm. L was tested and found to be large enough to prevent finite-size artifacts. Periodic boundary conditions were applied in all space directions. The long-range electrostatic interactions are corrected with standard Ewald sums with a cutoff in real space $R_{\mathrm{cut}} = L/2 = 11$ nm and reduced Ewald splitting parameter $\alpha^* = 3.0$ with error in F_{C} of around 10^{-6} kJ mol^{-1}[84]. The simulations consisted of 10^6 to 10^7 MC steps, with thermal equilibration of 10^5 MC steps. Typical runs lasted from 1 to 8 days using the Idun cluster (Norwegian University of Science and Technology, NTNU)[85], depending on the total particle number, which ranged from 50 to 1300. In each MC step, the following trial moves are performed: (i) translation of a particle (protein beads, crowder particles, ions); (ii) translation of the IDP chain as a whole; (iii) pivot rotation of a chain section of the IDP chain; (iv) slithering of the IDP chain, where a section of the chain is moved to the other end of the chain, mimicking the reptation of a snake; (v) protonation/deprotonation of an acid/basic bead of the IDP chain. The charge of a counter-ion is accordingly changed to maintain the system electroneutrality; and (vi) rotation of the crowders. The increment in the free energy is computed and the standard Metropolis algorithm applied: the trial configuration is always accepted if $\Delta F \leq 0$ and it is accepted with a probability equal to $\exp(-\beta\Delta F)$ otherwise.

The sought thermal averages were the average charge of a specific residue type A, $\langle q_{\mathrm{A}} \rangle$; the binding capacitance of A[36,86,87], $\langle c_{\mathrm{A}} \rangle$, defined as

$$\langle c_{\mathrm{A}} \rangle = \left(\frac{\partial q_{\mathrm{A}}}{\partial \mu_{\mathrm{A}}} \right) = \left\langle q_{\mathrm{A}}^2 \right\rangle - \langle q_{\mathrm{A}} \rangle^2 , \qquad (8)$$

the protein average charge Q

$$Q = \sum_{A}^{G} N_{\mathrm{A}} \langle q_{\mathrm{A}} \rangle , \qquad (9)$$

where N_{A} is the number of ionizable groups of type A among the G different types of acid/base groups; the global IDP binding capacitance, given by[36,86,87]

$$C = \frac{\partial Q}{\partial \mu} = \sum_{A}^{G} N_{\mathrm{A}} \left(\frac{\partial \langle q_{\mathrm{A}} \rangle}{\partial \mu} \right) = \sum_{A}^{G} N_{\mathrm{A}} c_{\mathrm{A}}. \qquad (10)$$

Finally, we also computed the radius of gyration R_g, which reads

$$R_g^2 = \sum_{i,j}^M \frac{1}{2M^2}(r_i - r_j)^2. \tag{11}$$

where r_i is the position of bead i and M is the number of beads of the IDP.

3 Results and discussion

3.1 Histatin-5 and β-amyloid titration in absence of crowders

Let us firstly discuss the ionization and conformational properties of histatin-5 and β-amyloid 42 in absence of crowder agents. The average protein charge Q as a function of the pH-value is shown in Figs. 3a (histatin-5) and 3b (β-amyloid 42) at added salt concentrations ranging from $c_s = 0$ (no added salt) to $c_s = 0.5$ M. Since we only add 1:1 salts, c_s can be directly identified with the ionic strength I. Note that in calculating I in this way the concentration of ions H^+ and OH^- coming from water self-ionization, which could be significant at very low and high pH-values, are neglected. However, as it will be seen, at these pH-values the influence of the ionic strength is very weak, so that we can identify I as the added salt concentration quite accurately.

It can be observed that histatin-5 essentially behaves as a polybase with average charge ranging from $+15$ to -2 and an isoeletric point pI close to 10.5, due to the presence of 15 basic but only 5 acidic groups. The pI-value of Histatin-5 is in good agreement with previous theoretical and computational calculations[88–91] Conversely, β-amyloid 42 contains eight acidic and seven basic groups, and exhibits an amphoteric behaviour. Its charge ranges from $+7$ to -8 with pI ~ 5, which is consistent with the observed self-aggregation of this protein at pH values close to 5[92]. The obtained histatin-5 titration curves agree reasonably well with previous work[50], where the average charge was computed using Semi-Grand Canonical Monte Carlo simulations with implicit ions using the Debye-Hückel potential. This mean field approximation is known to fail when increasing the ionic strength[93,94], so that moderate deviations from our computations are found at low pH-values for ionic strength larger than 0.1 M.

Clearly, the impact of the added salt on the titration curves is much more pronounced in the case of histatin-5, while it is very weak for β-amyloid 42. This point is better discussed by computing the increment in the charge due to the addition of salt at concentration c_s, i.e., $\Delta Q(c_s) = |Q(c_s)| - |Q(0)|$, shown in Figs. 3c (histatin-5) and 3d (β-amyloid 42). It can be observed that in general $\Delta Q(c_s)$ increases with c_s. This is not surprising since the added salt screens the electrostatic repulsion between equally-charged aminoacids along the chain favoring ionization[34,35]. Moreover, $\Delta Q(c_s)$ is larger for histatin-5 than for β-amyloid 42. This is possibly a consequence of the more balanced composition of β-amyloid 42, since the increase in c_s screens both the attractive and the repulsive interactions.

The binding capacitance as a function of the pH value is plotted in Figs. 3e and 3f for histadin-5 and β-amyloid 42, respectively. Note that the maxima of C and $\Delta Q(c_s)$ (panels c and d) take place at the same pH values, with pH $\simeq pK_{a,i}$ of the most

abundant amioacids, that is, histidine for histatin-5 and aspartic and glutamic acid for β-amyloid 42. Therefore, the salt screening effect is maximum for pH-values in which the protein charge regulation and fluctuation are maxima (recall that capacitance and fluctuations are directly linked, see Eqn. 10)[36,86,87]. It can be also observed that for histatin-5 the maxima of C are higher and shifted towards larger pH values as c_s increases. This behavior is also found in weak polyelectrolytes[36,50]. The capacitance and charge increment $\Delta q_A(c_s) = |q_A(c_s)| - |q_A(0)|$ for each individual amino acid type as a function of the pH and c_s can be found in the Supporting Information[†] (Figs. S1 and S2).

The radii of gyration R_g as a function of pH and salt concentration are presented in Figs. 4a (histatin-5) and 4b (β-amyloid 42). It can be observed that for histatin-5, R_g decreases as the pH increases (panel a), while, for β-amyloid 42, R_g exhibits a minimum around pH $= 5$ (panel b). This fact can be easily explained: at the isoelectric point (pI) of the IDPs (pI ~ 10.5 for histatin-5 and pI ~ 5 for β-amyloid 42) the aminoacids of the proteins are either neutral or perfectly balanced, and, as a result, the repulsive electrostatic intramolecular interactions are minimized and the protein is, on average, more compact. The increase in c_s from zero (squares) to 0.5 M (diamonds) generally leads to a decrease in the R_g. Again, the presence of salt screens the intramolecular interactions, leading to less extended conformation. This effect is more pronounced at pH values far from the isoelectric point. Interestingly, for pH-values close to pI, the situation is reversed and R_g slightly increases with the ionic strength of the medium. In this case, the intramolecular attractive electrostatic forces seems to be more important than their repulsive counterpart.

3.2 Charge regulation of IDPs in crowded media with neutral obstacles

Let us now populate the system with neutral crowders with the same geometrical properties as BSA. For simplicity, all results shown in this section refer to systems with constant salt concentration $c_s = 0.1$ M, except otherwise stated. We have also performed computations at $c_s = 0.01$ M, with similar results, which are reported as Suplementary Information[†] (Fig. S3). The titration curves of histatin-5 and β-amyloid 42 were calculated at different excluded volume fractions ϕ, defined as

$$\phi = \frac{4\pi N_C R_C^3}{3L^3}, \tag{12}$$

where $R_C = 2.73$ nm is the hard-core radius of the crowders, $L = 22$ nm is the length of the simulation box and N_c is the number of crowder particles, which ranges from 2 to 63. Note that the outer soft shell of the crowders can be penetrated, specially at high crowder concentrations[21], which is the reason why only the hard-core radius is considered in Eq. 12.

The effect of macromolecular crowding in the ionization properties of the IDPs is quantified by means of the difference between the absolute charges with and without crowding $\Delta Q'(\phi) = |Q(\phi)| - |Q(0)|$ where $Q(\phi)$ is the average charge of the protein at a given ϕ value. $\Delta Q'(\phi)$ is shown in Figs. 5a (histatin-5) and 5b (β-amyloid 42) as a function of the pH at ϕ-values ranging from:
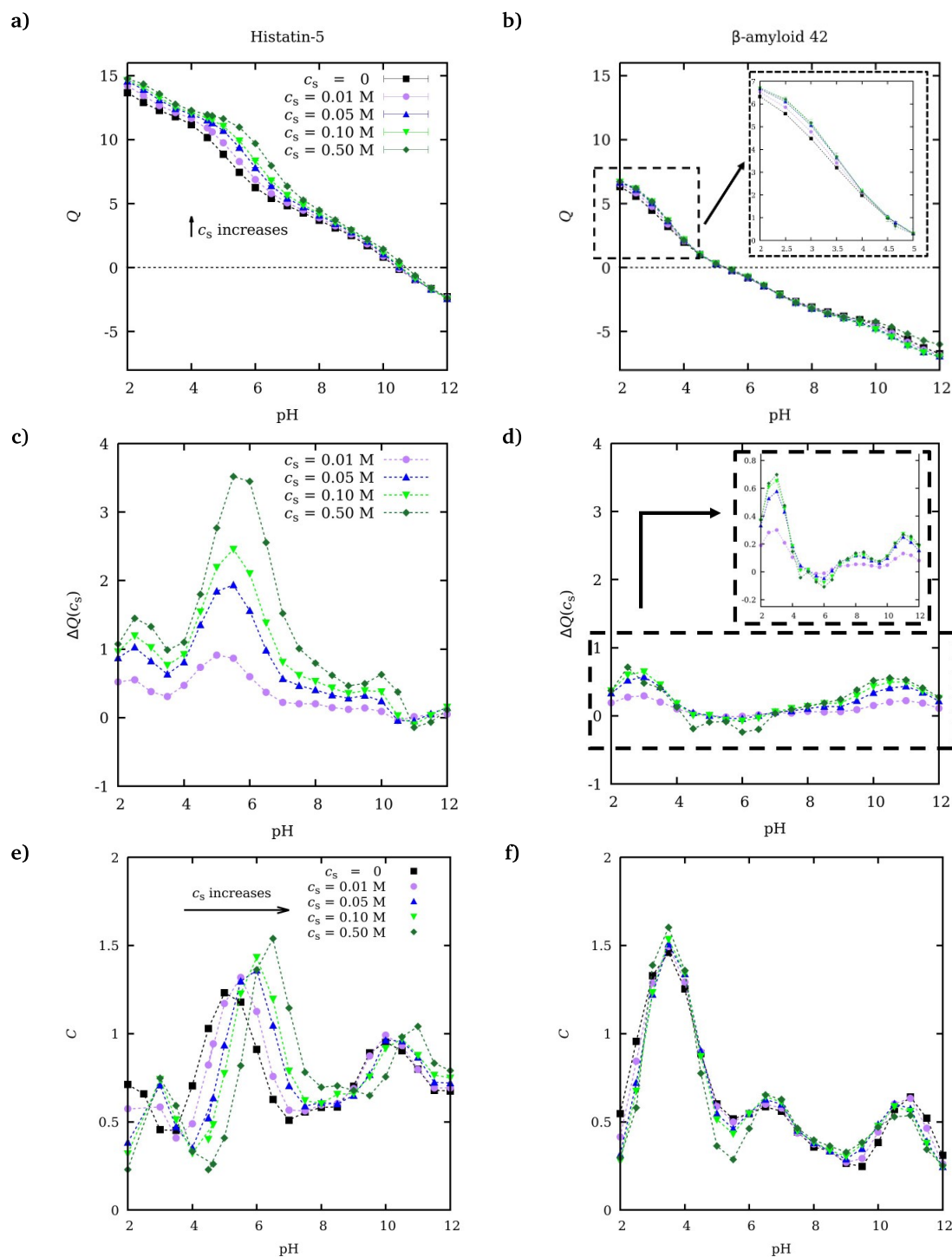
Fig. 3 Panels a) and b) show the average charge Q of the IDPs; panels c) and d) the charge increment due to the added salt $\Delta Q(c_s) = |Q(c_s)| - |Q(0)|$; and panels e) and f) the binding capacities C. The panels on the left-hand side refer to histatin-5 while the ones on the right to β-amyloid 42. The concentration of added salt are: no added salt (squares), $c_s = 0.01$ M (circles), 0.05 M (triangles), 0.1 M (inverted triangles) and 0.5 M (diamonds).
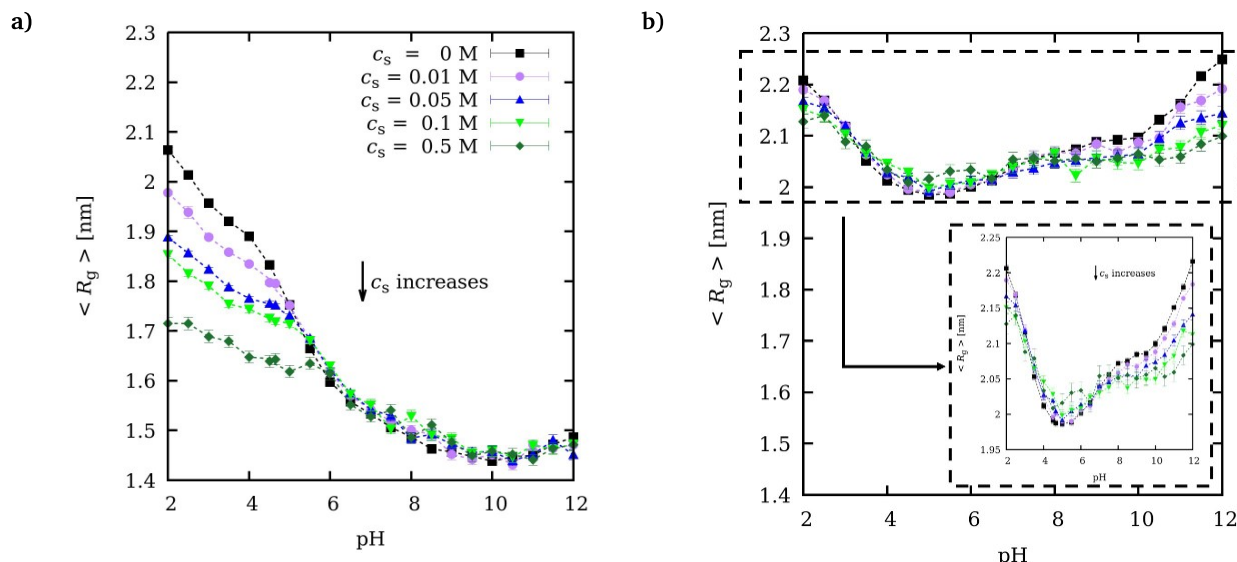
Fig. 4 Radius of gyration R_g of (a) histatin-5 and (b) β-amyloid 42 at salt concentrations ranging from $c_s = 0$ M (no added salt) to $c_s = 0.5$ M. The markers are the same as in Fig. 3.

$\phi = 0.1$ to $\phi = 0.5$. It can be observed that the impact of crowding is very different for the two studied IDPs. The average charge of histatin-5 increases with the crowder concentration at all the pH range, with a maximum increase of 0.6 units at pH = 6. Only for systems at pH = 11, a small decrease in the average charge observed. Conversely, β-amyloid 42 (Fig. 5b), presents a titration behavior that is nearly insensitive to the crowder concentration. It is only observed a small increase with ϕ at pH = 3 and pH = 10 and a small decrease at pH values from 4 to 7. The $\Delta Q'(\phi)$ *vs.* ϕ curves have been found to be very well fitted to an empiric power law in all the pH-range for both IDPs (See Section S4 in the Supporting Information[†]).

We also analyze the dependence of the average charge per aminoacid type q_A with ϕ by calculating the difference in charge with and without crowders $\Delta q'_A(\phi) = |q_A(\phi)| - |q_A(0)|$, where $q_A(\phi)$ is the average charge of an aminoacid type A at a given ϕ-value. In Figs. 5c (histatin-5) and 5d (β-amyloid 42), $\Delta q'_A(\phi)$ for aspartic acid (ASP), histidine (HIS) and lysine (LYS) are shown. These aminoacids are chosen as representatives of residues with acidic, neutral and basic isoeletric points, respectively. It can be observed that crowding affects the protonation/deprotonation of the aminoacids differently and $\Delta q'_A(\phi)$ of ASP, HIS, and LYS strongly depend on the identity of the IDP protein.

Interestingly, the variation of Q can be achieved by neutralizing aminoacids whose charges have opposite sign to that of the macromolecular charge. For instance, if an acidic residue, negatively charged, gets protonated, the global charge becomes more positive. An example can be observed at pH = 3, where both IDPs experience global charge increase (Figs. 5a and 5b), but the (absolute) charge of their acidic groups decrease (ASP in the Figs.5c and 5d). Note that at this pH only the charge of the acidic residues is affected by crowding, because pH$\simeq$p$K_{a,i} \simeq 3$. This is, again, the pH region where their binding capacitance, and consequently the charge regulation ability of ASP, exhibits a maximum

(see Fig. S5 in the Supporting Information[†]). As discussed in the previous subsection, the maxima and minima in $\Delta Q'(\phi)$ coincide with the peaks in the charge capacitance C, as observed in Fig. 5e and Fig. 5f.

Hypothetically, the dependence of the macromolecular charge on ϕ could be regulated by two possible mechanisms. On the one side, larger excluded volumes lead to increase in the effective ionic strength I' of the solution (same number of salt ions in a reduced accessible volume). For a system with N charged chemical species, I' can be expressed in terms of the crowder excluded volume fraction ϕ as

$$ I'(\phi) = \frac{1}{2} \sum_{i=1}^{N} c'_i(\phi) z_i^2 = \frac{c_s}{(1-\phi)}, \qquad (13) $$

where $c'_i(\phi)$ is the "effective" concentration of the chemical specie i with charge z_i. For instance, for $\phi = 0.5$ and $c_s = 0.1$ M the effective ionic strength is $I' = 0.2$ M. As a result, the intra-molecular electrostatic interactions are weaker since they are more screened, and the average protein charge should be affected.[34–36] On the other hand, in most of cases, excluded volume is found to induce more compact protein conformations.[5,7,8] This compaction of the IDPs reduces the distance between charged groups and thus increases the intra-molecular electrostatic interactions.

Let us assess the relative importance of these two possible mechanisms. With this aim let us take as a reference situation $c_s = 0.1M$. For $\phi = 0.5$, the effective ionic strength is $I' = 0.2$. If the variation in the IDPs charge is only due to the increase of I' induced by crowding, the corresponding charge variation in presence of crowding

$$ \Delta Q'(\phi = 0.5) = |Q(\phi = 0.5, c_s = 0.1\text{M})| - |Q(\phi = 0, c_s = 0.1\text{M})| \qquad (14) $$
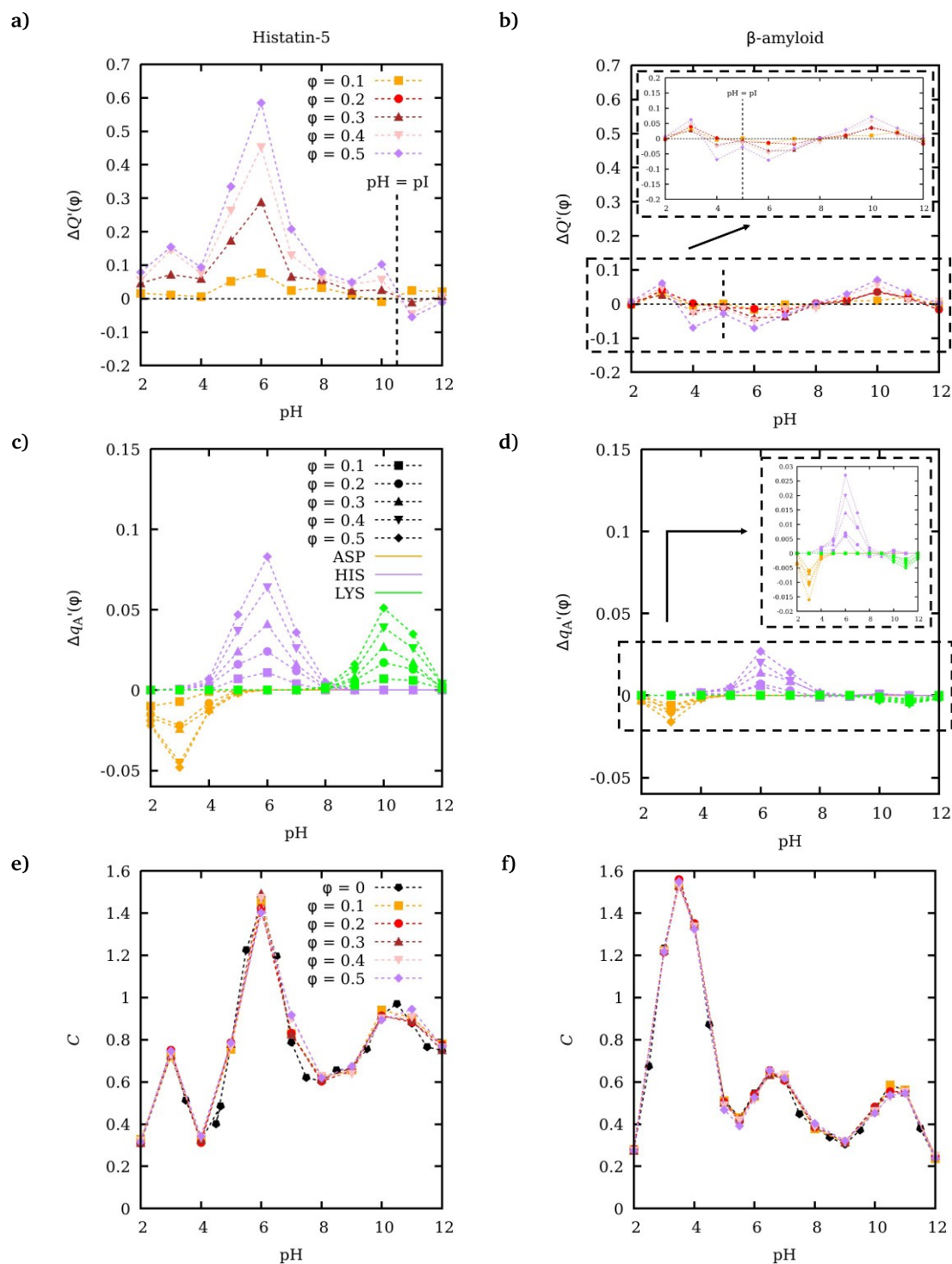
Fig. 5 Panels a and b: variation in the absolute macromolecular charge due to the presence of neutral crowders, $\Delta Q'(\phi) = |Q(\phi)| - |Q(0)|$. Panels c and d: variation in the average charge per aminoacid, $\Delta q'_A(\phi) = |q_A(\phi)| - |q_A(0)|$. Panels e and f: binding capacitance, C. Panels on the left-hand side refer to histatin-5 and the ones on the right-hand side to β-amyloid 42. The added salt concentration is $c_s = 0.1$ M of NaCl in all the simulations, while ϕ ranges from 0.1 to 0.5. The meaning of the markers and color of the lines used can be read inside the panels.
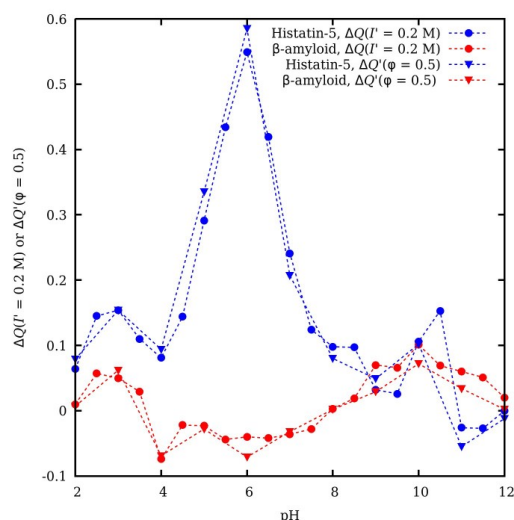
Fig. 6 Comparison between: i) charge variation produced when the added salt concentration is incremented from $c_s = 0.1$ M to 0.2 M without crowders $\Delta Q(I' = 0.2\text{M})$ (Eq. 15, circles); ii) charge variation produced when adding neutral crowders with resulting $\phi = 0.5$, $\Delta Q'(\phi = 0.5)$ (Eq. 14, triangles), to a protein solution with added salt concentration $c_s = 0.1$ M, i.e., with effective ionic strength $I' = 0.2$ M. Blue color refers to histatin-5 while red color refers to β-amyloid. As can be observed, $\Delta Q'(\phi = 0.5) \approx \Delta Q(I' = 0.2\text{M})$ evidencing that the main effect of the crowders is to increment the effective ionic strength.

should be the same as the charge variation without crowding but taking $c_s = I'$

$$\Delta Q(I' = 0.2\text{M}) = |Q(\phi = 0, c_s = 0.2\text{M})| - |Q(\phi = 0, c_s = 0.1\text{M})|,$$ (15)

that is

$$\Delta Q'(\phi = 0.5) \approx \Delta Q(I' = 0.2\text{M})$$ (16)

This comparison is shown in Fig. 6. Clearly $\Delta Q(I' = 0.2\text{M})$ and $\Delta Q'(\phi = 0.5)$ are very similar for all the range of pH-values. This result strongly suggests that the main mechanism by which neutral crowders affect the charge regulation is increasing the effective ionic strength. Conversely, it seems that protein compaction induced by macromolecular crowding does not affect the IDPs charge.

Figs. 7a (histatin-5) and 7b (β-amyloid 42) show the normalized radii of gyration, $R_g(\phi)/R_g(0)$, where $R_g(0)$ is the radius of gyration in absence of crowders, at different pH and ϕ values. It can be seen that it slightly decreases with ϕ. This is in good agreement with the results obtained by Kang and co-authors[95], which found a reduction of the macromolecule dimension due to the presence of crowders of comparable size. They proposed to fit the normalized R_g to the scaling law[95,96]

$$R_g(\phi)/R_g(0) = (1 - c\lambda\phi)^{1/5},$$ (17)

where $\lambda = R_g(0)/R_c$ is the ratio between the IDP radii of gyration without crowders $R_g(0)$ and the crowder compact radius R_c, and c is an empiric parameter to be fitted. In this work, λ was found
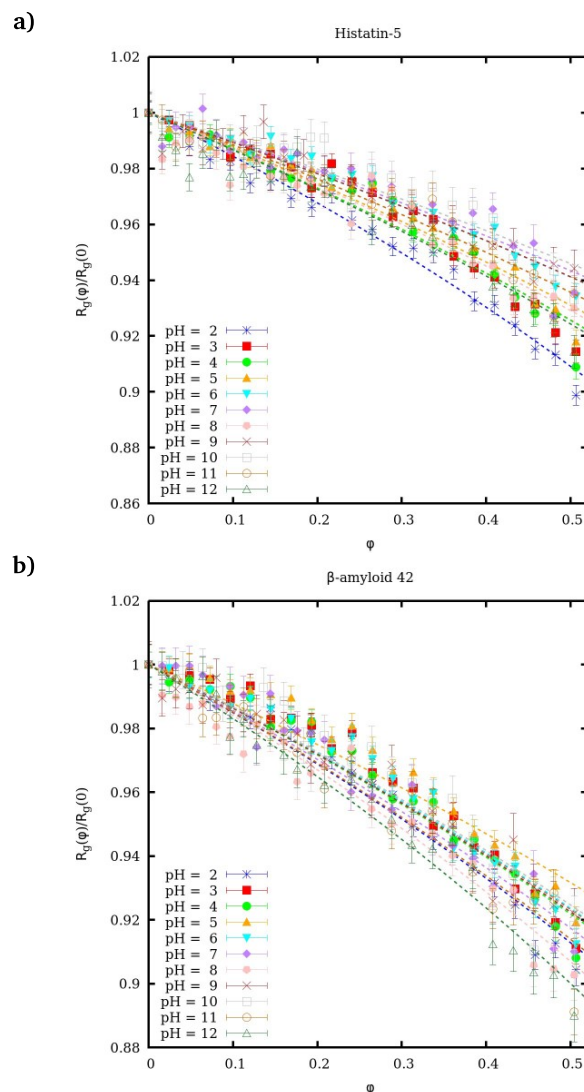
a)

b)

Fig. 7 Normalized radius of gyration, R_g, of (a) histatin 5 and (b) β-amyloid 42 *vs.* ϕ at pH-values ranging from 2 to 12 in the presence of neutral crowders. Dashed lines represent the best-fit to the scaling law (Eq. 17).

to range from 5.4 to 8.0, depending on the IDP and the pH conditions. The best fit curves to Eq. (17), are depicted as dashed lines in the Figs. 7a and 7b. The corresponding c-values (listed in Section S6 as Supporting Information[†]), are found to be nearly independent of the IDP and the pH value, with $c \simeq 0.09$ in all the cases. It is also worth mentioning that if λ is set to 1, following the approach used in Ref.[53], where the crowders were IDPs, we obtain c-values for histatin-5 around ~ 0.6, close to the reported value $c = 0.71$ for similar salt conditions.

3.3 IDPs titration in presence of charged crowders

The charged crowders are here modeled as a coarse grained version of Bovine Serum Albumin (BSA) proteins, which we assume to have the same characteristic radii (R_C and R_H) than the neutral crowders of the previous sub-section. The only difference is that we incorporate ionized groups at the surface, modeled as charged beads which mimic the ionized groups of the protein. The total charge of the surface corresponds to the average charge of BSA at the pH-value and salt concentration of the simulation. The latter information, shown in Tab. 2, is taken from Ref. [70], where the average charge of BSA for $c_s = 0.01$ M in a wide range of pH-values was experimentally determined. The charge of the crowders is compensated by the corresponding counter-ions in order to maintain the electroneutrality of the solution. We restrict ourselves to ϕ values up to 0.2 due to two reasons: (i) for very acidic/basic pH values the number of counter-ions increases dramatically with ϕ making the computations prohibitively expensive and (ii) the presence of charged hard beads in the crowder surface increases the excluded volume, which complicates the equilibration of systems at large ϕ-values.

Following the same order as in the previous sub-section, let us firstly analyze the variation in the IDP charge induced by the presence of charged crowders, $\Delta Q'(\phi) = |Q(\phi)| - |Q(0)|$, depicted in Figs. 8a (histatin 5) and 8b (β-amyloid 42). The average charges of the specific residues $\Delta q'_A(\phi) = |q_A(\phi)| - |q_A(0)|$ are reported in Figs. 8c and 8d. The simulations are performed at four ϕ-values: 0.05 (triangles), 0.1 (squares), 0.15 (inverted triangles) and 0.2 (circles). It can be observed that, for the same pH and ϕ values, charged crowders induce significantly larger variation in the charge of the individual aminoacids and in the IDP global charge. For example, for $\phi = 0.2$, histatin-5 exhibits a maximum $\Delta Q'(\phi)$ value of 0.2 units (pH = 6) with neutral crowders while in the presence of charged crowders the maximum $\Delta Q'(\phi)$ is 0.75. Likewise, for β-amyloid 42, $\Delta Q'(\phi)$ is very small for neutral crowders but increases significantly for almost all pH range with charged crowders. Again, the $\Delta Q'(\phi)$ vs. ϕ curves have been found to be very well fitted to an empiric power law in all the pH-range for both IDPs (See Section S4 in the Supporting Information[†]). The binding capacitance C in the presence of charged crowders is presented in Figs. 8e and 8f. It can be seen that crowding produces the shift of the first maximum towards larger pH values for histatin-5. A small increase in the height of the first maximum (at pH = 4) for β-amyloid 42 is also found. The same trend can be observed in the binding capacitance per aminoacid (Supporting Information[†], Fig. S7).

Note that, as happened with neutral crowders, in some cases (mostly at acidic pH-values), the protein charge increases by reducing the charge of the aminoacids with charge sign being opposite to the global charge. This fact can be observed, for example, at pH = 3 in Figs. 8a and 8c. Curiously, this phenomenon takes place for almost all the pH range in the case of β-amyloid 42 (See Figs. 8b and 8d). Note also that, for β-amyloid 42, the dependence of Δq_A of HIS with pH depends of the nature of the crowder. In the presence of neutral crowders, its charge slightly increases for larger ϕ values (See Fig. 5d), while the opposite situation is

observed for charged crowders.

In the previous sub-section, we highlighted that a fundamental mechanism of charge regulation upon the addition of neutral crowders was the increment of the effective ionic strength I' due to the reduction of the available volume. This effect should be even larger if the crowders are charged due to the presence of the counter-ions associated to them. I' can now be calculated by modifying Eq. 13 in order to include the counter-ions coming from the crowders. The resulting effective ionic strength I' reads

$$I'(\phi, \text{pH}) = \frac{c_s}{(1-\phi)} + \frac{3\phi|z(\text{pH})|}{4\pi R_c^3 N_A(1-\phi)}, \tag{18}$$

where $z(\text{pH})$ is the crowder charge at a given pH value (see Tab. 2), R_c is the crowder hard-core radius (we take $R_c = 2.73$ nm as in the previous sub-section) and N_A is the Avogadro number. The second term on the right-hand side represents the contribution of the counter-ions coming from the charged crowders. I' vs. ϕ curves (Eq. 18) for $c_s = 0.01M$ at different pH-values can be found as Supporting Information[†] (see Section S8). Depending on ϕ and pH, I' may amount to as much as 0.18 M, almost twenty times the c_s-value.

As in the previous section, let us investigate if the main mechanism for the IDP's charge regulation is the increment in I'. We want to compare the resulting charge variation $\Delta Q(I' = 0.02\text{M})$, calculated in the same way as in Eq. 15, with that of a system with charged crowders whose effective ionic strength is always $I' = 0.02$M, independently of the pH-value. That means that, for each pH-value, we have to calculate the ϕ-value for which Eq. 18 predicts $I' = 0.02$ M. The comparison between the charge variations in both situations, $\Delta Q(I' = 0.02\text{M})$ and $\Delta Q'(\phi)$, is shown in Fig. 9. As in the case of neutral crowders, both charge variations are very similar, evidencing that the main effect of the charged crowders is to increment the ionic strength. However, in this case it can be observed a shift between $\Delta Q(c_s)$ and $\Delta Q'(\phi)$ values which was not detected for neutral crowders (Fig. 6). This fact suggests that there is a significant contribution to charge regulation from the electrostatic interaction between the IDP and the charged crowders. This observation is in good agreement with previous research on the interactions between weak polyelectrolytes and charged nanoparticles, where the titration curves of weak polyelectrolytes was observed to be shifted as the surface charge of the nanoparticle increased[97]. This effect seems to be, however, more modest for IDP's than for polyelectrolytes, probably because the charge density is smaller in the case of IDP's. The same analysis has been performed for $I' = 0.05$ M, i.e. larger excluded volumes, which is reported as Supporting Information[†] (see Section S9). The resulting shift is less pronounced in this case, suggesting that effect of increasing I' is now more pronounced and the IDP-charged crowder interaction plays a minor role. However, further research would probably be necessary to fully clarify this point.

The normalized radius of gyration R_g, as a function of ϕ for pH ranging from 3 to 11 is depicted in Figs. 10a and 10b. It is found that increasing ϕ leads to a slight decrease in R_g of both IDPs. This fact can be in part due to the steric hindrance caused by the presence charged crowders, which also took place in the case
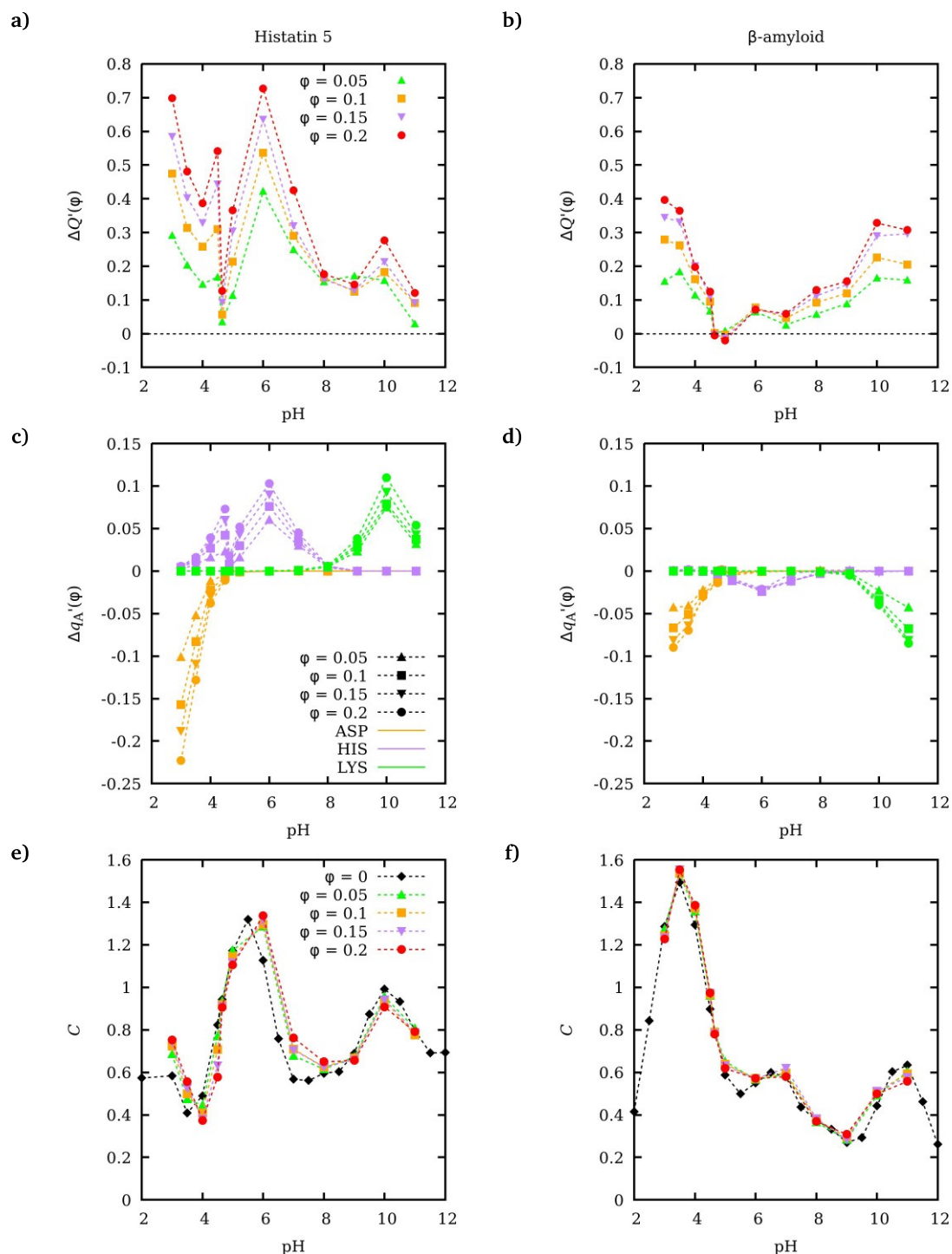
Fig. 8 Panels a and b: variation in the absolute macromolecular charge due to the presence of charged crowders, $\Delta Q'(\phi) = |Q(\phi)| - |Q(0)|$; panels c and d: variation in the average charge per aminoacid, $\Delta q'_A(\phi) = |q_A(\phi)| - |q_A(0)|$; and panels e and f: binding capacitance C. Panels on the left-hand side refer to histatin-5 and the ones on the right-hand side to β-amyloid 42. The added salt concentration is $c_s = 0.01$ M of NaCl in all the simulations, while ϕ ranges from zero to 0.2. The meaning of the markers and color of the curves can be read inside the panels.
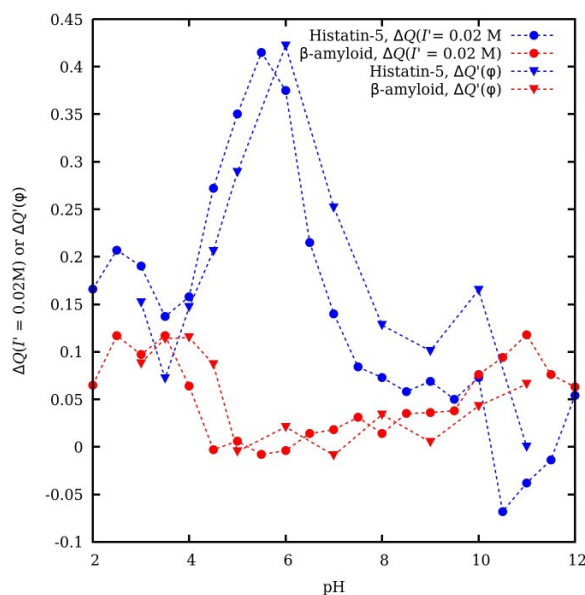
Fig. 9 Comparison between: i) charge variation produced when the added salt concentration is incremented from $c_s = 0.01$ M to 0.02 M without crowders ($\Delta Q(I' = 0.02\text{M}) = |Q(\phi = 0, c_s = 0.02\text{M})| - |Q(\phi = 0, c_s = 0.01\text{M})|$, circles); and ii) charge variation produced when adding charged crowders $\Delta Q'(\phi)$ (triangles) to a protein solution with added salt concentration $c_s = 0.01$ M. The excluded volume $\phi(pH, 0.01M)$ is chosen such as the effective ionic strength I' (calculated using Eq.18) is always $I' = 0.02$ M. Blue color refers to Histatin-5 while red color refers to β-amyloid.

of neutral crowders. However, for the same ϕ, this effect is much stronger in the presence of charged crowders, as one concludes by comparing the normalized R_g *vs.* ϕ curves obtained with neutral (Figs. 7a and 7b) and with charged crowders. The difference is specially remarkable for histatin-5 at pH-values between pH = 3 and pH = 4, in which histatin-5 is highly charged. This difference can be explained again by the fact that increasing charged crowder concentration produces an extra increase in the effective ionic strength of the media, which weakens electrostatic repulsion and facilitates protein compaction. The normalized R_g obtained by the simulations (markers) have been fitted to the scaling law in Eq. 17 (dashed lines) and the resulting c-values are listed in Section S6 in the Supporting Information[†]). In general, very good fitting is obtained, with c-values ranging from 0.08 to 0.33. For pH values close to the IDPs isoelectric points (5 and 11 for histatin-5 and β-amyloid 42, respectively), the obtained c-values are similar to those corresponding to neutral crowders. Away from the isoelectric point, however, the resulting c-values for charged crowders are larger than those calculated in the presence of neutral crowders, specially for histatin-5 in the range pH = 3 to pH = 4.

4 Conclusions

The effect of macromolecular crowding in the charge regulation of two Intrinsically Disordered Proteins (IDPs), histatin-5 and β-amyloid 42, is studied by means of Semi-Grand Canonical Monte Carlo simulations. It is found that the titration curve of histatin-5 depends on the salt concentration. This effect is specially remarkable at pH-values for which the binding capacitance presents a maximum, *i.e.* the protein charge is more susceptible
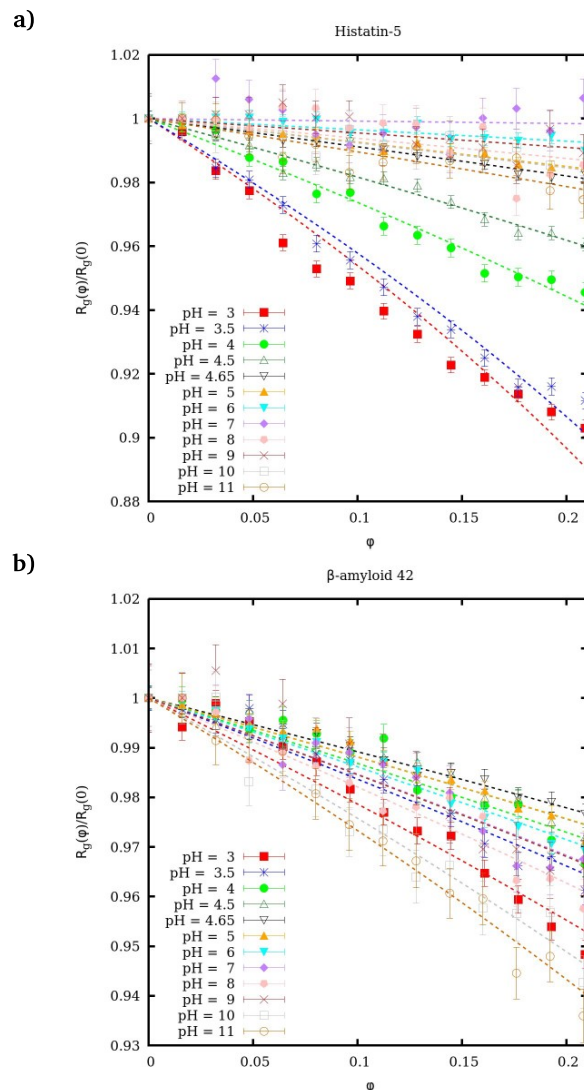
a)

b)

Fig. 10 Normalized radius of gyration, R_g, of (a) histatin 5 and (b) β-amyloid 42 *vs.* ϕ at pH-values ranging from 2 to 12 in the presence of charged crowders. Dashed lines represent the best fit to the scaling law (Eq. 17).

to be regulated. Conversely, the titration curve of β-amyloid 42 was nearly insensitive to salt concentration, probably due to its polyampholyte nature: repulsive and attractive intra-molecular forces are affected in opposite way. The radius of gyration R_g of the IDPs is significantly salt dependent for pH values far from their isoelectric point pI. In this case, R_g is reduced as the salt concentration increases, due to screening of the intra-molecular electrostatic repulsion.

Our results suggest that the main mechanism by which neutral crowders change the IDP charge is the effective increase in salt concentration due to excluded volume (which screens the IDP charge). The presence of neutral crowders induces charge regulation on histatin-5 whereas the charge of β-amyloid 42 is nearly unaffected. This can be again probably explained by the fact that in histatin-5 the positively charged basic residues are predominant. Conversely, β-amyloid 42 is a polyampholyte, and repulsive and attractive forces are affected in opposite manner.

The situation changes when charged crowders are introduced. For both IDPs, the global charge increases with ϕ for almost all the pH range. In this case, the effect of crowding in the IDPs charge is found to be not only dependent on the increase in the effective ionic strength, resulting from the volume reduction and the addition of counter-ions associated to the charged crowders, but also due to their direct interaction with the charged crowders, causing a shift when compared to the systems in absence of charged crowding agents at the same ionic strength.

For both neutral and charged crowders, the analysis of the average charge per aminoacid type reveals that, in some cases (specially at acidic pH-values), the mechanism through which the IDP regulates its global charge consists of neutralizing the charge of the aminoacids with charge sign opposite to that of the global charge. Moreover, the pH values for which the charge is more affected by crowding coincide with those of the maximum binding capacitance. Finally, the radius of gyration R_g decreases with ϕ, and its dependence on ϕ fits very well the power low proposed in the Ref.[95], containing only one fitting parameter.

We highlight that, even though the charge regulation of the IDPs induced by macromolecular crowding can be in principle considered moderate, it could have relevant biological implications. For example, charge regulation due to macromolecular crowding could be relevant in membrane-less organelles, which are formed by charged macromolecules.[98] Furthermore, the physicochemical effects here discussed could be probably more intense in systems with larger charge densities (polycarboxylates, polyamines, polysaccharides) or in the presence of multi-valent ions. It is worth to mention that in our simulations the salt concentration is kept constant. This situation resembles an *in vitro* experiment, where the titration of the IDP is performed in presence of a buffer at constant salt concentration. Alternatively, one could perform simulations at constant salt chemical potential, which could be more convenient, for instance, in describing dialysis experiments. Further work is necessary to clarify this point. To our knowledge, the present work represents the first attempt to study, at least by computational simulation, the interplay between charge regulation and macromolecular crowding.

Conflicts of interest

There are no conflicts to declare.

Acknowledgements

Notes and references

1 J.-P. Behr, *The lock-and-key principle: the state of the art-100 years on*, J. Wiley, 1994.

2 J. J. Ward, J. S. Sodhi, L. J. McGuffin, B. F. Buxton and D. T. Jones, *Journal of Molecular Biology*, 2004, **337**, 635–645.

3 V. N. Uversky, *Journal of Biomedicine and Biotechnology*, 2010, **2010**, 1–14.

4 V. N. Uversky, *Biochimica et Biophysica Acta - Proteins and Proteomics*, 2011, **1814**, 693–712.

5 A. V. Fonin, A. L. Darling, I. M. Kuznetsova, K. K. Turoverov and V. N. Uversky, *Cellular and Molecular Life Sciences*, 2018, **75**, 3907–3929.

6 V. N. Uversky and A. K. Dunker, *Biochimica et Biophysica Acta - Proteins and Proteomics*, 2010, **1804**, 1231–1264.

7 A. P. Minton, *Biopolymers*, 1981, **20**, 2093–2120.

8 A. P. Minton, *Biophysical Journal*, 1992, **63**, 1090–1100.

9 Y. Shen, J. M. Jacobs, D. G. Camp, R. Fang, R. J. Moore, R. D. Smith, W. Xiao, R. W. Davis and R. G. Tompkins, *Analytical Chemistry*, 2004, **76**, 1134–1144.

10 T. C. Laurent, *European Journal of Biochemistry*, 1971, **21**, 498–506.

11 R. J. Ellis, *Trends in Biochemical Sciences*, 2001, **26**, 597–604.

12 D. S. Banks and C. Fradin, *Biophysical Journal*, 2005, **89**, 2960–2971.

13 P. Mereghetti and R. C. Wade, *Journal of Physical Chemistry B*, 2012, **116**, 8523–8533.

14 J. Balbo, P. Mereghetti, D. P. Herten and R. C. Wade, *Biophysical Journal*, 2013, **104**, 1576–1584.

15 C. Balcells, I. Pastor, E. Vilaseca, S. Madurga, M. Cascante and F. Mas, *Journal of Physical Chemistry B*, 2014, **118**, 4062–4068.

16 I. Pastor, L. Pitulice, C. Balcells, E. Vilaseca, S. Madurga, A. Isvoran, M. Cascante and F. Mas, *Biophysical Chemistry*, 2014, **185**, 8–13.

17 C. Balcells, I. Pastor, L. Pitulice, M. Via, S. Madurga, E. Vilaseca, A. Isvoran, M. Cascante and F. Mas, *New Frontiers in Chemistry*, 2015, **24**, 3–16.

18 S. Kondrat, O. Zimmermann, W. Wiechert and E. V. Lieres, *Physical Biology*, 2015, **12**, 46003.

19 P. M. Blanco, M. Via, J. L. Garcés, S. Madurga and F. Mas, *Entropy*, 2017, **19**, 105.

20 M. Feig, I. Yu, P. H. Wang, G. Nawrocki and Y. Sugita, *Journal of Physical Chemistry B*, 2017, **121**, 8009–8025.

21 P. M. Blanco, J. L. Garcés, S. Madurga and F. Mas, *Soft Matter*, 2018, **14**, 3105–3114.

22 A. Kuzmak, S. Carmali, E. von Lieres, A. J. Russell and S. Kondrat, *Scientific Reports*, 2019, **9**, 1–7.

23 E. A. Cino, M. Karttunen and W. Y. Choy, *PLoS ONE*, 2012, **7**, e49876.

24 C. P. Brangwynne, P. Tompa and R. V. Pappu, *Nature Physics*, 2015, **11**, 899–904.

25 A. Banks, S. Qin, K. L. Weiss, C. B. Stanley and H. X. Zhou, *Biophysical Journal*, 2018, **114**, 1067–1079.

26 G. L. Dignon, W. Zheng, Y. C. Kim, R. B. Best and J. Mittal, *PLoS Computational Biology*, 2018, **14**, 1–23.

27 F. C. Zegarra, D. Homouz, A. G. Gasic, L. Babel, M. Kovermann, P. Wittung-Stafshede and M. S. Cheung, *Journal of Physical Chemistry B*, 2019, **123**, 3607–3617.

28 R. K. Das and R. V. Pappu, *Pnas*, 2013, **110**, 13392–13397.

29 R. K. Das, K. M. Ruff and R. V. Pappu, *Current opinion in structural biology*, 2015, **32**, 102–112.

30 M. Ullner and B. Jonsson, *Macromolecules*, 1996, **29**, 6645–6655.

31 S. Ulrich, M. Seijo and S. Stoll, *The Journal of Physical Chemistry B*, 2007, **111**, 8459–8467.

32 J. L. Garcés, S. Madurga and M. Borkovec, *Physical Chemistry Chemical Physics*, 2014, **16**, 4626–4638.

33 J. L. Garcés, S. Madurga, C. Rey-Castro and F. Mas, *Journal of Polymer Science, Part B: Polymer Physics*, 2017, **55**, 275–284.

34 P. M. Blanco, S. Madurga, F. Mas and J. L. Garcés, *Polymers*, 2018, **10**, 811.

35 P. M. Blanco, S. Madurga, F. Mas and J. L. Garcés, *Macromolecules*, 2019, **52**, 8017–8031.

36 P. M. Blanco, S. Madurga, C. F. Narambuena, F. Mas and J. L. Garcés, *Polymers*, 2019, **11**, 1962.

37 S. Uyaver and C. Seidel, *Europhysics Letters*, 2003, **64**, 536–542.

38 S. T. Whitten, B. Garcia-Moreno E. and V. J. Hilser, *Proceedings of the National Academy of Sciences*, 2005, **102**, 4282–4287.

39 D. S. Olander and A. Holtzer, *Journal of the American Chemical Society*, 1968, **90**, 4549–4560.

40 H. Boroudjerdi, Y. Kim, A. Naji, R. R. Netz, X. Schlagberger and A. Serr, *Physics Reports*, 2005, **416**, 129–199.

41 M. Muthukumar, *Macromolecules*, 2017, **50**, 9528–9560.

42 J. Landsgesell, L. Nová, O. Rud, F. Uhlík, D. Sean, P. Hebbeker, C. Holm and P. Košovan, *Soft Matter*, 2019, **15**, 1155–1185.

43 A. F. Jorge, R. S. Dias and A. A. Pais, *Biomacromolecules*, 2012, **13**, 3151–3161.

44 C. F. Narambuena, E. P. Leiva and E. Pérez, *Colloids and Surfaces A: Physicochemical and Engineering Aspects*, 2015, **487**, 49–57.

45 S. K. Ramisetty and R. S. Dias, *Journal of Molecular Liquids*, 2015, **210**, 64–73.

46 M. Stornes, P. Linse and R. S. Dias, *Macromolecules*, 2017, **50**, 5978–5988.

47 P. Torres, L. Bojanich, F. Sanchez-Varretti, A. J. Ramirez-Pastor, E. Quiroga, V. Boeris and C. F. Narambuena, *Colloids and Surfaces B: Biointerfaces*, 2017, **160**, 161–168.

48 M. Stornes, B. Shrestha and R. S. Dias, *Journal of Physical Chemistry B*, 2018, **122**, 10237–10246.

49 P. B. Torres, E. Quiroga, A. J. Ramirez-pastor, V. Boeris and C. F. Narambuena, *The Journal of Physical Chemistry B*, 2019, **123**, 8617–8627.

50 K. Hyltegren, T. Nylander, M. Lund and M. Skepö, *Journal of Colloid and Interface Science*, 2016, **467**, 280–290.

51 K. Hyltegren and M. Skepö, *Journal of Colloid and Interface Science*, 2017, **494**, 266–273.

52 C. Cragnell, E. Rieloff and M. Skepö, *Journal of Molecular Bi-ology*, 2018, **430**, 2478–2492.

53 E. Fagerberg, S. Lenton and M. Skepö, *Journal of Chemical Theory and Computation*, 2019, **15**, 6968–6983.

54 A. M. Baptista, V. H. Teixeira and C. M. Soares, *The Journal of Chemical Physics*, 2002, **117**, 4184–4200.

55 J. Mongan, D. A. Case and J. A. McCammon, *Journal of Computational Chemistry*, 2004, **25**, 2038–2048.

56 B. J. MacKay, L. Denepitiya, V. J. Iacono, S. B. Krost and J. J. Pollock, *Infection and Immunity*, 1984, **44**, 695–701.

57 J. J. Pollock, L. Denepitiya, B. J. MacKay and V. J. Iacono, *Infection and Immunity*, 1984, **44**, 702–707.

58 S. Puri and M. Edgerton, *Eukaryotic Cell*, 2014, **13**, 958–964.

59 K. Wróblewski, R. Muhandiram, A. Chakrabartty and A. Bennick, *European Journal of Biochemistry*, 2001, **268**, 4384–4397.

60 A. Bennick, *Critical Reviews in Oral Biology and Medicine*, 2002, **13**, 184–196.

61 J. Kang, H. G. Lemaire, A. Unterbeck, J. M. Salbaum, C. L. Masters, K. H. Grzeschik, G. Multhaup, K. Beyreuther and B. Müller-Hill, *Nature*, 1987, **325**, 733–736.

62 P. M. Gorman, C. M. Yip, P. E. Fraser and A. Chakrabartty, *Journal of Molecular Biology*, 2003, **325**, 743–757.

63 G. F. Chen, T. H. Xu, Y. Yan, Y. R. Zhou, Y. Jiang, K. Melcher and H. E. Xu, *Acta Pharmacologica Sinica*, 2017, **38**, 1205–1235.

64 R. Jurij and L. Per, *Journal of Computational Chemistry*, 2015, **36**, 1259–1274.

65 F. G. Oppenheim, T. Xu, F. M. McMillian, S. M. Levitz, R. D. Diamond, G. D. Offner and R. F. Troxler, *Journal of Biological Chemistry*, 1988, **263**, 7472–7477.

66 Y. Nozaki and C. Tanford, *Methods in Enzymology*, 1967, **11**, 715–734.

67 J. L. Garcés, G. J. M. Koper and M. Borkovec, *J. Phys. Chem. B*, 2006, **110**, 10937–10950.

68 P. Vilaseca and G. Franzese, *Journal of Chemical Physics*, 2010, **133**, 1–11.

69 F. Leoni and G. Franzese, *Journal of Chemical Physics*, 2014, **141**, 174501.

70 M. K. Menon and A. L. Zydney, *Analytical Chemistry*, 1998, **70**, 1581–1584.

71 J. Bernhardt and H. Pauly, *Journal of Physical Chemistry*, 1975, **79**, 584–590.

72 J. R. Whitaker, *Analytical Chemistry*, 1963, **35**, 1950–1953.

73 M. L. Huber, R. A. Perkins, A. Laesecke, D. G. Friend, J. V. Sengers, M. J. Assael, I. N. Metaxa, E. Vogel, R. Mareš and K. Miyagawa, *Journal of Physical and Chemical Reference Data*, 2009, **38**, 101–125.

74 A. K. Gaigalas, J. B. Hubbard, M. McCurley and S. Woo, *Journal of Physical Chemistry*, 1992, **96**, 2355–2359.

75 T. Raj and W. H. Flygare, *Biochemistry*, 1974, **13**, 3336–3340.

76 F. Carlsson, M. Malmsten and P. Linse, *Journal of the American Chemical Society*, 2003, **125**, 3140–3149.

77 Y. Xu, M. Mazzawi, K. Chen, L. Sun and P. L. Dubin, *Biomacromolecules*, 2011, **12**, 1512–1522.

78 R. De Vries, *J. Chem. Phys.*, 2014, **120**, 3475–3481.

79 Y. Cemil, J. Heyda, M. Ballauff and J. Dzubiella, *J. Chem. Phys.*, 2015, **143**, 064905.

80 C. Yigit, M. Kanduc, M. Ballau and J. Dzubiella, *Langmuir*, 2017, **33**, 417–427.

81 M. J. Blandamer and M. C. Symons, *Journal of Physical Chemistry*, 1963, **67**, 1304–1306.

82 S. Madurga, A. Martín-Molina, E. Vilaseca, F. Mas and M. Quesada-Pérez, *Journal of Chemical Physics*, 2007, **126**, 234703–1–234703–11.

83 S. Madurga, C. Rey-Castro, I. Pastor, E. Vilaseca, C. David, J. L. Garcés, J. Puy and F. Mas, *Journal of Chemical Physics*, 2011, **135**, 184103.

84 B. Linse and P. Linse, *Journal of Chemical Physics*, 2014, **141**, 184114.

85 M. Själander, M. Jahre, G. Tufte and N. Reissmann, *EPIC: An Energy-Efficient, High-Performance GPGPU Computing Research Infrastructure*, 2019.

86 E. D. Cera, *J. Phys. Chem.*, 1991, **95**, 5082–5086.

87 M. Lund and B. Jo, *Quarterly Reviews of Biophysics*, 2013, **46**, 265–281.

88 E. J. Helmerhorshmt, W. V. Hof, P. Breeuwer, E. C. I. Veer-man, T. Abee, R. F. Troxler, A. V. N. Amerongen and F. G. Oppenheim, *The Journal of Biological Chemistry*, 2001, **276**, 5643–5649.

89 H. Nikawa, H. Fukushima, S. Makihira, T. Hamada and L. P. Samaranayake, *Oral diseases*, 2004, **10**, 221–228.

90 A. Kurut, J. Henriques, J. Forsman, M. Skepo and M. Lund, *Proteins*, 2014, **82**, 657–667.

91 C. Cragnell, D. Durand, B. Cabane and M. Skepo, *Proteins*, 2016, 1–15.

92 G. M. Klug, D. Losic, S. S. Subasinghe, M. I. Aguilar, L. L. Martin and D. H. Small, *European Journal of Biochemistry*, 2003, **270**, 4282–4293.

93 L. Guldbrand, B. Jönsson, H. Wennerström and P. Linse, *The Journal of Chemical Physics*, 1984, **80**, 2221–2228.

94 M. Borkovec, B. Jönsson and G. J. M. Koper, *Surface and Colloid Science*, 2001, 99–339.

95 H. Kang, P. A. Pincus, C. Hyeon and D. Thirumalai, *Physical Review Letters*, 2015, **114**, 068303:1–5.

96 D. Thirumalai, *Physical Review A*, 1988, **37**, 269–276.

97 A. Laguecir and S. Stoll, *Polymer*, 2005, **46**, 1359 – 1372.

98 W. Stroberg and S. Schnell, *Journal of Theoretical Biology*, 2017, **434**, 42–49.
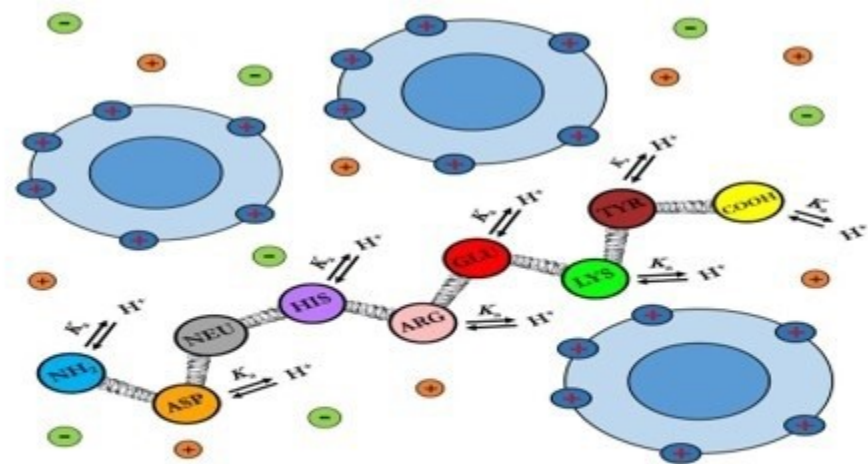
The coupling between ionization and conformational properties of two IDPs, histatin-5 and β-amyloid 42, in the presence of neutral and charged crowders is studied performing Semi-Grand Canonical Monte Carlo simulations where the IDPs charge is a dynamic property, undergoing protonation/deprotonation processes.

79x51mm (150 x 150 DPI)